A helical shaped broadband circularly polarized dielectric resonator antenna

A Helical Shaped Broadband Circularly Polarized Dielectric Resonator Antenna

ARTICLE HISTORY
Compiled July 8, 2020

ABSTRACT
By modifying the shape of a rectangular dielectric resonator antenna (DRA), a wideband circularly polarized (CP) radiator is introduced. The modified structure is composed of two L-shaped dielectric pieces stacked onto each other. The resulting geometry is similar to a two-turn helix with a rectangular cross section. Placing a coaxial probe adjacent to the sidewall of the DRA excites multiple orthogonal modes in the antenna which in sequence leads to a wideband CP DRA. The special geometry of the DRA provides the required quadrature phase difference between the orthogonal components of the electric fields. The measured input scattering parameter, $|S_{11}|$, is below - 10 dB from 3 to 4.6 GHz (42%). Also, the frequency band in which axial ratio (AR) is lower than 3dB extends from 3.1 to 3.83 GHz (21.07%), which is suitable for WIMAX applications. The measured results of the fabricated prototype are presented to verify the simulations.

KEYWORDS
Circularly Polarized (CP), Dielectric Resonator Antenna, Wideband Response.

1. Introduction

Dielectric resonator antennas (DRAs) have been the topic of many research studies due to their specific features like wide bandwidth, small size, and high efficiency [1-4]. Early works on DRAs have mainly been devoted to the linearly polarized (LP) DRAs. However, due to the advantages of the circularly polarized (CP) antennas over the LP ones, including the minimization of polarization loss and fading, a major part of the research on DRAs is nowadays focused on CP DRAs [5-10]. In LP communication systems, the losses of the polarization mismatch arise because of the reception of the signal from different paths and misalignment of the antenna, which can be stopped by introducing circular polarization. Generally speaking, there are two feeding mechanisms for the generation of CP modes in the DRAs, namely (i) single-feed and (ii) dual-feed mechanisms. Compared to the dual-feed method, the single-feed technique is relatively simple from the manufacturing point of view, whereas the dual-feed method usually has a wider axial ratio (AR) bandwidth. However, by changing the shape of the antenna, multiple orthogonal degenerate modes could be excited in the DRA, which in turn increases the AR bandwidth of the singly-fed configuration. For example, the application of a stair-shaped DRA as the radiator in [8] produced a wide AR bandwidth of 22%. Moreover, in [11], a spidron fractal shaped DRA with the AR bandwidth of 11.57% has been reported. A broadband CP DRA with a trapezoidal shape has been studied in [12], and another instance has been examined in [13], in which four sequentially rotated metallic plates were placed around the DRA to increase its AR bandwidth. Also, in [14], a planar feed has been employed to excite CP modes in an

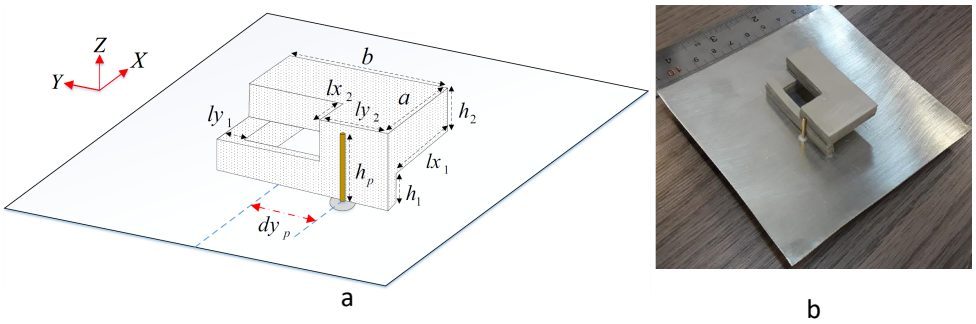

Figure 1. The configuration of the proposed DRA. (a) 3D view (b) the fabricated prototype.

omnidirectional DRA: The excitation of the $TM_{01\delta}$ and $TE_{011+\delta}$ modes is responsible for CP operation. In [15], a high gain circularly polarized DRA has been reported, in which the parasitic elements are responsible for the directive radiation characteristics. A dualband circularly polarized rectangular DRA has been proposed in [16], where the DRA has been excited by using triangular ring-shaped aperture.

In this work, a modified rectangular DRA with a broad impedance and AR bandwidth is presented. The proposed DRA is constructed by stacking two L-shaped dielectric pieces onto each other. The structure obtained by this method can support multiple orthogonal modes required for the generation of circular polarization. Additionaly, it also produces the quadrature phase difference between the orthogonal components of the electric fields. The antenna parameters are varied to find the best responses of the matching and AR.

In the following, the operation mechanism of the proposed antenna is explained by plotting the electric field distributions of the modes responsible for the wideband CP response. The measurements results of the fabricated prototype are compared with those of the simulation, and a reasonable agreement between them is observed.

2. Antenna Configuration

Figure 1 displays the layout of CP DRA (Fig. 1a) and the photograph of the fabricated prototype (Fig. 1b). The antenna consists of two L-shaped dielectric pieces with different sizes and the same permittivity of $\varepsilon_r = 10.2$ rotated by 180° with respect to each other and stacked onto each other. These dielectric pieces are mounted on a metallic ground plane with the lateral size of 10cm × 10cm. The resulting structure is similar to a two-turn helix with a rectangular cross section. As shown in Fig. 1, the coaxial probe feed with the height of h_p and offset of dy_p from the center of the antenna in the y-direction is utilized to excite the modes in the DRA. The optimized parameters for the resultant geometry are as follows: $a = 25.2$mm, $b = 43.3$mm, $l_{x1} = 22.2$mm, $l_{x2} = 11.9$mm, $l_{y1} = 6.7$mm, $l_{y2} = 18$mm, $h_1 = h_2 = 7.62$mm, $dy_p = 7.9$mm and $h_p = 12.3$mm.

The antenna is simulated using the Ansoft HFSS and CST MWS. The fabricated antenna, illustrated in Fig. 1(b), is measured and its results are presented in the following section.

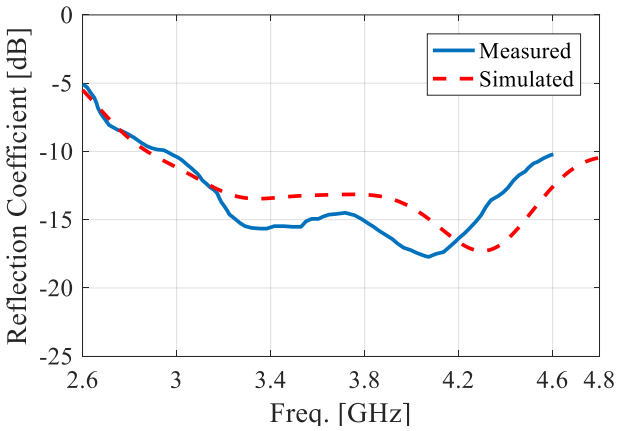

Figure 2. The measured and simulated input scattering parameter,$|S_{11}|$, of the proposed DRA.

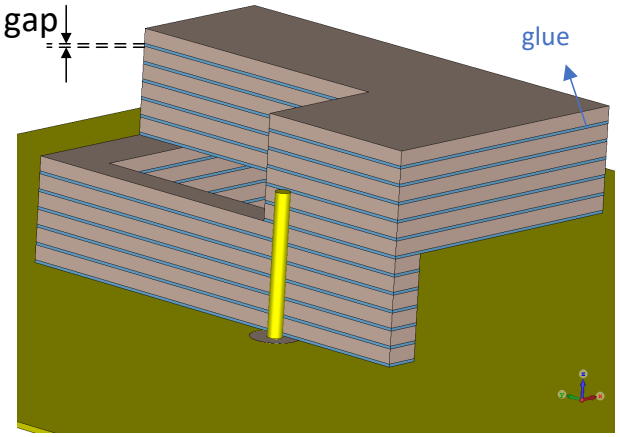

Figure 3. The perspective view of the DRA.

3. Results and discussion

Figure 2 depicts the measured and simulated results of the input scattering parameter of the proposed antenna. A good impedance match across the frequency band of 3GHz to 4.6GHz is observed. Note that, the discrepancy between the simulated and measured data originates from the errors in the fabrication process of the antenna. Because of the limited equipment in our laboratory, both L-shaped dielectric pieces are constructed by placing Rogers 6010 sheets with the standard thickness of 1.27mm onto each other. To fix the structure, an adhesive material with the dielectric constant of $\varepsilon_r = 2.2$ is used [25]. Hence, as shown in Fig. 3, the glue layers between the dielectric layers cause a discrepancy between simulation and experiment. However, such dissimilarities are also observed in the literature [8, 17, 18]. Figure 4 shows the effect of the glue layers on the input scattering parameter of the DRA. As reported in [25], the glue layer thickness is determined to be 0.1 mm. Note that the level of $|S_{11}|$ is considerably affected.

Figure 5 displays the measured and simulated results of the axial ratio of the DRA. The measured results indicate that the AR frequency band ($AR < 3dB$) starts from

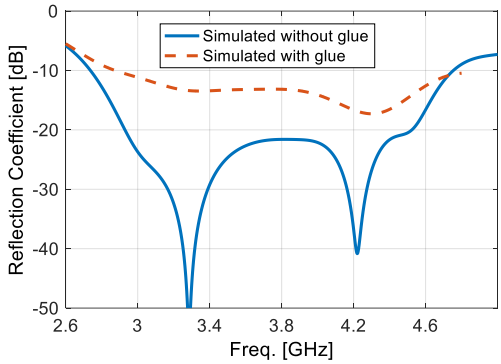

Figure 4. The simulated reflection coefficient of the antenna with and without the adhesive material between the layers, $gap = 0.1$ mm.

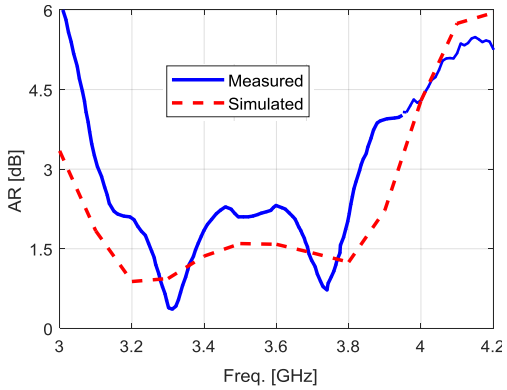

Figure 5. The measured and simulated axial ratio (AR) of the antenna.

3.1GHz. It is very close to that predicted by the simulation (3.16GHz). However, by assuming the threshold value of 3dB for the maximum acceptable AR, the simulated and measured AR bandwidths are 26% (3.03 − 3.94GHz) and 21.07% (3.1 − 3.83GHz), respectively. Observe that the measured AR response has better level than that of the simulation at some frequencies. As can be seen in the literature [22], [19], [24], In some cases, this may happen.

Figure 6 illustrates the measured and simulated right hand CP (RHCP) gain of the antenna in the boresight direction, $\theta = 0$. Observe that the measured RHCP gain is higher than 5dB across the antenna bandwidth, reaching 6.4dB at 3.4GHz.

In order to specify the modes responsible for the wideband CP performance of the antenna, the electric field distributions at different frequencies are plotted in Figs. 7 and 8. The top and 3D views of the E-field distributions at 3.3GHz with the phase angles of $-45°$and $45°$ are plotted in Fig. 7. Observe that the electric field distributions in Figs. 7(a) and (b) look similar to that of the TE^x_{111} mode, and the electric fields in Figs. 7(c) and (d) resemble that of the TE^y_{111} mode.

Therefore, the TE^x_{111} and TE^y_{111} modes are the orthogonal degenerate modes responsible for CP operation at 3.3 GHz. Using the dielectric waveguide model (DWM)[2] and by including the effective permittivity ε_{eff}[5], the resonant frequencies of the TE^x_{111} and TE^y_{111} modes can be calculated. For this purpose, it is assumed that the dielectric pieces and air form a rectangular box with the dimensions of $a \times b \times (h_1 + h_2)$. So, the

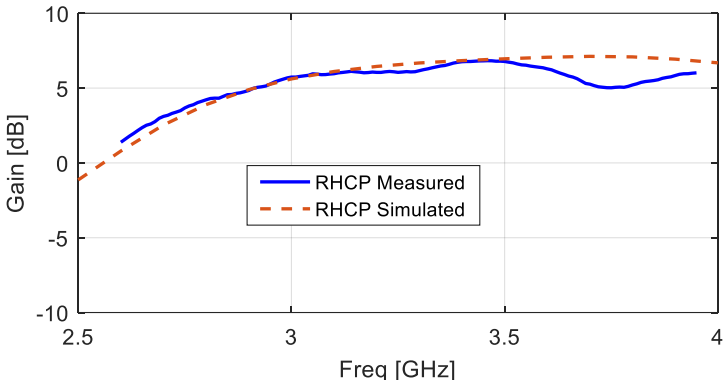

Figure 6. The measured and simulated RHCP gains of the antenna.

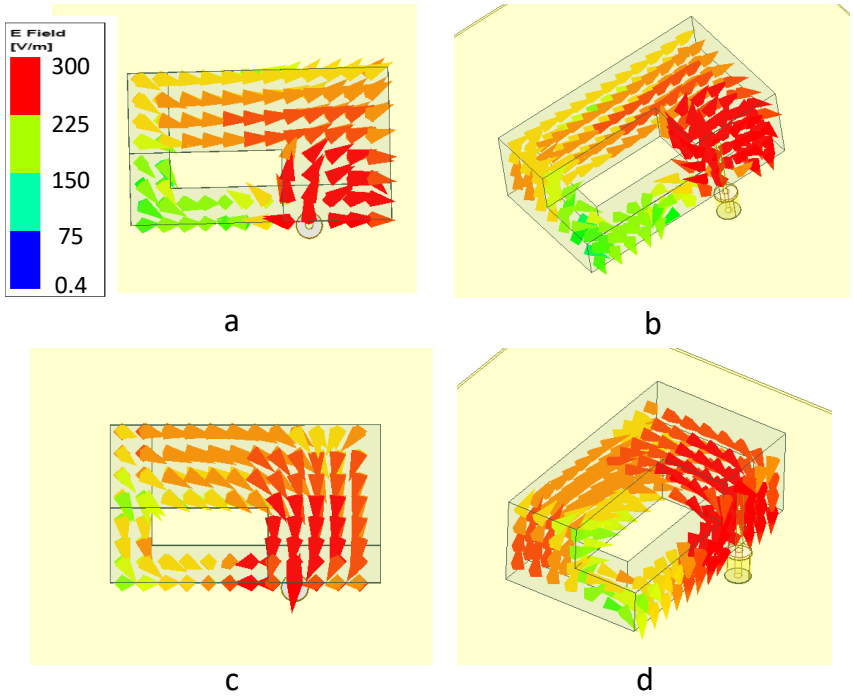

Figure 7. The Electric field distribution of the proposed antenna at 3.3GHz. (a) TE^{x}_{111} mode, -45°, top view (b) TE^{x}_{111} mode, -45°, 3D view (c) TE^{y}_{111} mode, 45°, top view (d) TE^{y}_{111} mode, 45°, 3D view.

effective permittivity of the block fitted in this box can be determined using[5]:

$$\varepsilon_{eff} = \frac{\varepsilon_{Air} V_{Air} + \varepsilon_{Dielectric} V_{Dielectric}}{V_{Air} + V_{Dielectric}} \tag{1}$$

where $\varepsilon_{Dielectric} = 10.2$ and $V_{Dielectric} = ab(h_1 + h_2) - lx_1\,(b - ly_1)\,h_1 - lx_2(b - ly_2)h_2$ are the permittivity and volume of the helical shaped structure, and $\varepsilon_{Air} = 1$ and $V_{air} = lx_1\,(b - ly_1)\,h_1 + lx_2(b - ly_2)h_2$ are the permittivity and volume of the air. Using this method the effective permittivity is calculated to be $\varepsilon_{eff} = 5.51$. For the

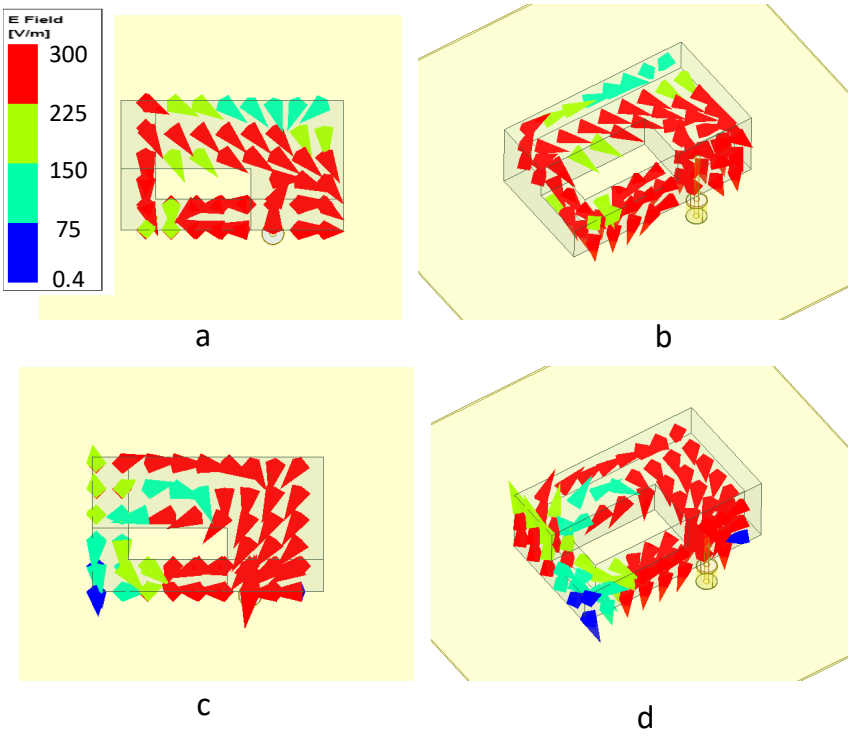

Figure 8. The Electric field distribution of the proposed antenna at 3.7GHz. (a) -45°, top view (b) -45°, 3D view (c) 45°, top view (d) 45°, 3D view.

TE^x_{111} mode, the resonant frequency can be calculated using [2]:

$$(\sqrt{\varepsilon_{eff}k_0^2 - k_y^2 - k_z^2}) \tan(\frac{b\sqrt{\varepsilon_{eff}k_0^2 - k_y^2 - k_z^2}}{2}) = \sqrt{k_y^2 + k_z^2 - k_0^2} \quad (2)$$

where $k_y = \pi/b$, $k_z = \pi/2(h_1 + h_2)$, $k_0 = 2\pi f_0/c$ and c is the speed of light in the vacuum. Also, the resonant frequency of TE^y_{111} mode is found using:

$$(\sqrt{\varepsilon_{eff}k_0^2 - k_x^2 - k_z^2}) \tan(\frac{b\sqrt{\varepsilon_{eff}k_0^2 - k_x^2 - k_z^2}}{2}) = \sqrt{k_x^2 + k_z^2 - k_0^2} \quad (3)$$

where $k_x = \pi/a$ and the other parameters are as mentioned for TE^x_{111} mode. The left and right sides of the eqs. (2) and (3) are plotted in the Figs. 9(a) and (b), respectively and the solutions to these equations are the intersections of these curves. As shown in Figs. 9(a) and (b), the resonant frequencies of the TE^x_{111} and TE^y_{111} modes are calculated to be 3.48 and 3 GHz, respectively, which are close to the location of the minimum of the AR curve in Fig. 5. Consequently, this method is useful for the prediction of the first guess of the resonant frequencies of these two modes.

As shown in Fig. 8, two hybrid modes stimulated using the coaxial probe are the origin of CP performance at 3.7GHz. The required conditions of the orthogonal com-

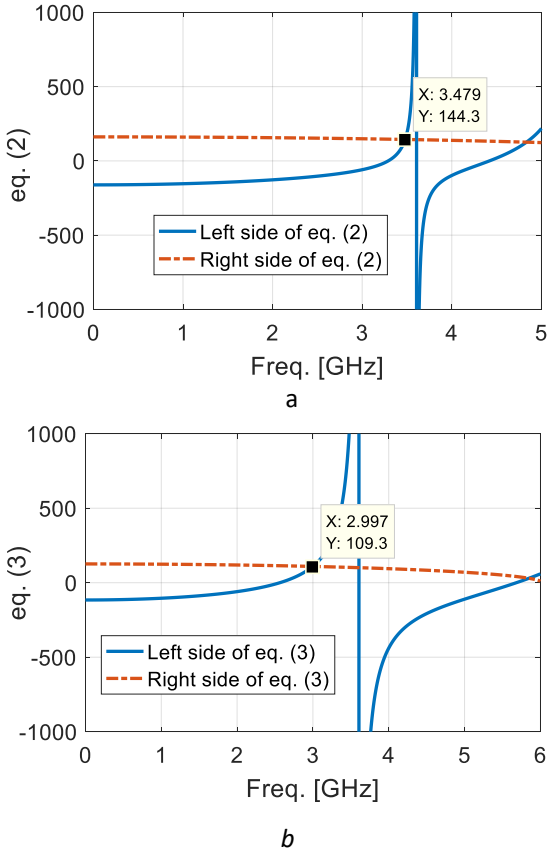

Figure 9. The graphical solution for the resonant frequencies of the DRA, (a) TE^{x}_{111} mode, (b) TE^{y}_{111} mode.

ponents of the electric fields and the quadrature phase difference between them can be produced by these degenerate modes. Furthermore, the presented scheme also allows a fine tuning of the resonant frequencies.

The measured and simulated far-field radiation patterns of the antenna at 3.2, 3.5 and 3.8 GHz are shown in Fig. 10. Note that, the levels of RHCP components are 19dB higher than those of the LHCP in the XoZ plane and in the boresight direction ($\theta = 0°$) at all frequencies. This value is 18.5dB in the YoZ plane at all frequencies. Also, observe that the proposed antenna provides a stable broadside radiation pattern across the operating frequency band. Note that for the pattern at 3.8 GHz in the YoZ plane, the RHCP and LHCP components have the same level at 30 deg, due to the excitation of the hybrid DRA modes. In fact, the special field distributions of these modes cause the unacceptable level of the cross polar discrimination in the angle of 30°. Still, it performs suitably up to 20°, where the difference between the levels of the RHCP and LHCP components is about 5 dB. Similar behavior has also been reported [6,28]. The agreement between the simulated and measured patterns is also observable. Figure 11 depicts the calculated radiation efficiency of the proposed antenna. It is above 95% for the complete bandwidth.

Finally, the proposed CP DRA is compared with some CP DRAs available in the literature, as listed in Table 1. Observe that the proposed structure provides better AR Bandwidth than those of [21] and [22]. Compared to [19] and [20], it has nearly

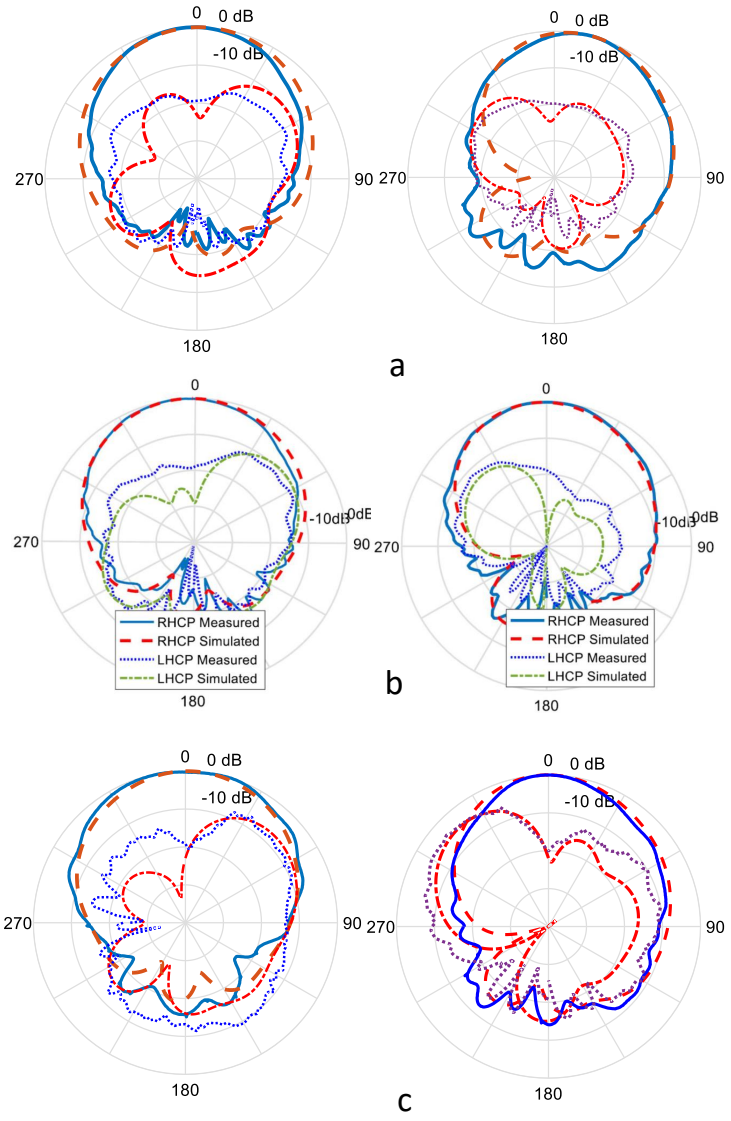

Figure 10. The measured and simulated results of the radiation patterns (a) at 3.2 GHz, (b) at 3.5 GHz, (c) at 3.8 GHz. Left: XZ plane (ϕ=0), Right: YZ plane (ϕ=90).

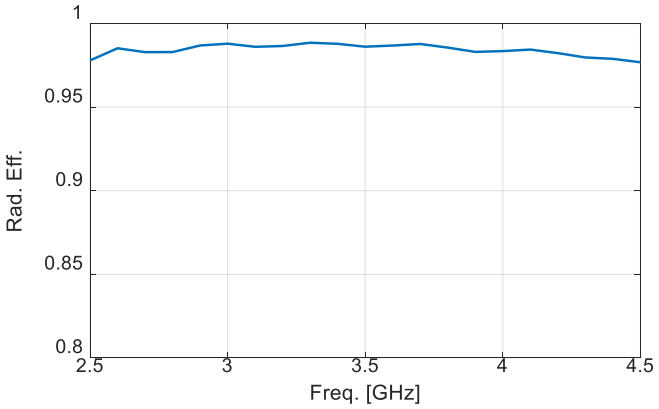

Figure 11. The simulated radiation efficiency of the proposed antenna.

Table 1. Performances of CP DRAs

Ref.	Techniques	Resonator Size	Axial Ratio Bandwidth	Impedance Bandwidth	Peak Gain [dB]	Efficiency
[17]	stacked DRA	$0.46\lambda_0 \times 0.46\lambda_0 \times 0.16\lambda_0$	22.8%	25.4%	7.7	90%
[18]	stacked and fed by SIW	$0.7\lambda_0 \times 0.55\lambda_0 \times 0.23\lambda_0$	27%	30%	7.5	89%
[19]	H-shaped strip fed DRA	$0.23\lambda_0 \times 0.35\lambda_0 \times 0.43\lambda_0$	9.6%	20.7%	5	-
[20]	cross slot fed irregular DRA	$0.22\lambda_0 \times 0.22\lambda_0 \times 0.24\lambda_0$	18.7%	25.9%	4.83	-
[21]	substrate integrated DRA	$1.15\lambda_0 \times 1.15\lambda_0 \times 0.13\lambda_0$	34.6%	30%	8.15	90%
This work	Helical shaped DRA	$0.29\lambda_0 \times 0.5\lambda_0 \times 0.18\lambda_0$	21.07%	42%	6.4	95%

similar AR bandwidth but lower resonator size and wider impedance bandwidth than both. Although the DRA in [23] has a better AR performance, its resonator size is much bigger than that of the our proposed antenna and its impedance bandwidth is not as wide as the present work.

4. Conclusion

By cutting two dissimilar rectangular cubes from a rectangular DRA, a new geometry is resulted, which is suitable for wideband CP applications. The wideband response of this antenna is because of the excitation of the multiple orthogonal modes in the DRA. This novel structure has an impedance bandwidth of 42% ($3 - 4.6$GHz) and an axial ratio bandwidth of 21.07% ($3.1 - 3.83$GHz). The proposed DRA is fabricated and its results agree reasonably well with those of the simulations.

Disclosure statement

No potential conflict of interest was reported by the author(s).

Funding

This work was supported by Iran Telecommunication Research Center.

References

[1] A. Petosa, and A. Ittipiboon, "Dielectric Resonator Antennas: A Historical Review and the Current State of the Art," *IEEE Antennas and Propagation Magazine*, vol. 52, no. 5, pp. 91-116, Oct. 2010.

[2] A. Petosa, *Dielectric Resonator Antenna Handbook* (Norwood, MA, Artech House, 2007).

[3] K. W. Leung, E. H. Lim and X. S. Fang, "Dielectric Resonator Antennas: From the Basic to the Aesthetic,"*Proceedings of the IEEE*, vol. 100, no. 7, pp. 2181-2193, July 2012.

[4] R. K. Mongia and P. Bhartia, "Dielectric resonator antennas—a review and general design relations for resonant frequency and bandwidth,"7 *International Journal of Microwave and Millimeter-Wave Computer-Aided Engineering*, vol. 4, no. 3, pp. 230–247, 1994.

[5] S. Fakhte, H. Oraizi and R. Karimian, "A Novel Low-Cost Circularly Polarized Rotated Stacked Dielectric Resonator Antenna," *IEEE Antennas and Wireless Propagation Letters*, vol. 13, pp. 722-725, 2014.

[6] A. Perron, T. A. Denidni and A. R. Sebak, "Circularly Polarized Microstrip/Elliptical Dielectric Ring Resonator Antenna for Millimeter-Wave Applications," *IEEE Antennas and Wireless Propagation Letters*, vol. 9, pp. 783-786, 2010.

[7] A. A. Abdulmajid, Y. Khalil and S. Khamas, "Higher-Order-Mode Circularly Polarized Two-Layer Rectangular Dielectric Resonator Antenna," *IEEE Antennas and Wireless Propagation Letters*, vol. 17, no. 6, pp. 1114-1117, June 2018.

[8] S. Fakhte, H. Oraizi, R. Karimian and R. Fakhte, "A New Wideband Circularly Polarized Stair-Shaped Dielectric Resonator Antenna," *IEEE Transactions on Antennas and Propagation*, vol. 63, no. 4, pp. 1828-1832, April 2015.

[9] M. Abedian, S. K. A. Rahim, S. Danesh, M. H. Jamaluddin and M. T. Islam, "Compact wideband circularly polarised dielectric resonator antenna," *Electronics Letters*, vol. 53, no. 1, pp. 5-6, 5 1 2017.

[10] L. Guo and K. W. Leung, "Compact Unilateral Circularly Polarized Dielectric Resonator Antenna," *IEEE Transactions on Antennas and Propagation*, vol. 66, no. 2, pp. 668-674, Feb. 2018.

[11] A. Altaf, Y. Yang, K. Lee and K. C. Hwang, "Circularly Polarized Spidron Fractal Dielectric Resonator Antenna," *IEEE Antennas and Wireless Propagation Letters*, vol. 14, pp. 1806-1809, 2015.

[12] Y. Pan, K. W. Leung, "Wideband circularly polarized trapezoidal dielectric resonator antenna", *IEEE Antennas and Wireless Propagation Letters*, vol. 9, pp. 588-591, 2010.

[13] M. Yang, Y. Pan and W. Yang, "A Singly Fed Wideband Circularly Polarized Dielectric Resonator Antenna," *IEEE Antennas and Wireless Propagation Letters*, vol. 17, no. 8, pp. 1515-1518, Aug. 2018.

[14] W. Li, K. W. Leung and N. Yang, "Omnidirectional Dielectric Resonator Antenna With a Planar Feed for Circular Polarization Diversity Design," *IEEE Transactions on Antennas and Propagation*, vol. 66, no. 3, pp. 1189-1197, March 2018.

[15] B. Bahreini, H. Oraizi, N. Noori and S. Fakhte, "Design of a Circularly Polarized Parasitic Array With Slot-Coupled DRA With Improved Gain for the 5G Mobile System," *IEEE Antennas and Wireless Propagation Letters*, vol. 17, no. 10, pp. 1802-1806, Oct. 2018.

[16] A. Gupta and R. K. Gangwar, "Dual-Band Circularly Polarized Aperture Coupled Rectangular Dielectric Resonator Antenna for Wireless Applications," IEEE Access, vol. 6, pp. 11388-11396, 2018.

[17] A. Motevasselian, A. Ellgardt, and B. L. G. Jonsson, "A circularly polarized cylindrical dielectric resonator antenna using a helical exciter," *IEEE Transactions on Antennas and Propagation*, vol. 61, no. 3, pp. 1439–1443, March 2013.

[18] L. C. Y. Chu, D. Guha, and Y. M. M. Antar, "Conformal strip-fed shaped cylindrical dielectric resonator: Improved design of a wideband wireless antenna," *IEEE Antennas and Wireless Propagation Letters*, vol. 8, pp. 482–485, 2009.

[19] W. Sun, W. Yang, P. Chu and J. Chen, "Design of a Wideband Circularly Polarized Stacked Dielectric Resonator Antenna," *IEEE Transactions on Antennas and Propagation*, vol. 67, no. 1, pp. 591-595, Jan. 2019.

[20] W. Yang, W. Sun, H. Tang and J. Chen, "Design of a Circularly Polarized Dielectric Resonator Antenna With Wide Bandwidth and Low Axial Ratio Values," *IEEE Transactions on Antennas and Propagation*, vol. 67, no. 3, pp. 1963-1968, March 2019.

[21] U. Illahi et al., "Design of New Circularly Polarized Wearable Dielectric Resonator Antenna for Off-Body Communication in WBAN Applications," *IEEE Access*, vol. 7, pp. 150573-150582, 2019.

[22] H. N. Chen, J. Song and J. Park, "A Compact Circularly Polarized MIMO Dielectric Resonator Antenna Over Electromagnetic Band-Gap Surface for 5G Applications," *IEEE Access*, vol. 7, pp. 140889-140898, 2019.

[23] M. Yang, Y. Pan, Y. Sun and K. Leung, "Wideband Circularly Polarized Substrate-Integrated Embedded Dielectric Resonator Antenna for Millimeter-Wave Applications," *IEEE Transactions on Antennas and Propagation*, vol. 68, no. 2, pp. 1145-1150, Feb. 2020.

[24] X. Fang, K. W. Leung and E. H. Lim, "Singly-Fed Dual-Band Circularly Polarized Dielectric Resonator Antenna," *IEEE Antennas and Wireless Propagation Letters*, vol. 13, pp. 995-998, 2014.

[25] S. Fakhte, L. Matekovits and I. Aryanian, "Rectangular Dielectric Resonator Antenna With Corrugated Walls," *IEEE Access*, vol. 7, pp. 3422-3429, 2019.

[26] Y. Ding, K. W. Leung and K. M. Luk, "Compact Circularly Polarized Dualband Zonal-Slot/DRA Hybrid Antenna Without External Ground Plane," *IEEE Transactions on Antennas and Propagation*, vol. 59, no. 6, pp. 2404-2409, June 2011.